GEOPHYSICAL RESEARCH LETTERS, VOL. 34, L21404, doi:10.1029/2007GL031840, 2007

Pore-scale spectral induced polarization signatures associated with FeS biomineral transformations

Lee Slater,[1] Dimitrios Ntarlagiannis,[1,2] Yves R. Personna,[1] and Susan Hubbard[3]

Received 29 August 2007; revised 2 October 2007; accepted 15 October 2007; published 13 November 2007.

[1] We measured spectral induced polarization (SIP) signatures in sand columns during (1) FeS biomineralization produced by sulfate reducing bacteria (*Desulfovibrio vulgaris*) under anaerobic conditions, and (2) subsequent biomineral dissolution upon return to an aerobic state. The low-frequency (0.1–10 Hz peak) relaxations produced during biomineralization can be modeled with a Cole-Cole formulation, from which the evolution of the polarization magnitude and relaxation length scale can be estimated. We find that the modeled time constant is consistent with the polarizable elements being biomineral encrusted pores. Evolution of the model parameters is consistent with FeS surface area increases and pore-size reduction during biomineral growth, and subsequent biomineral dissolution (FeS surface area decreases and pore expansion) upon return to the aerobic state. We conclude that SIP signatures are diagnostic of pore-scale geometrical changes associated with FeS biomineralization by sulfate reducing bacteria.
Citation: Slater, L., D. Ntarlagiannis, Y. R. Personna, and S. Hubbard (2007), Pore-scale spectral induced polarization signatures associated with FeS biomineral transformations, *Geophys. Res. Lett.*, *34*, L21404, doi:10.1029/2007GL031840.

1. Introduction

[2] Near surface geophysical measurements are potentially sensitive to microbial processes (see *Atekwana et al.* [2006] for review). Geophysics offers the possibility of observing microbial processes non-invasively, and at larger scales inaccessible with standard microbiological techniques. One microbial process detectable with electrical geophysical methods is iron sulfide (FeS) biomineralization induced by sulfate reducing bacteria [*Williams et al.*, 2005; *Ntarlagiannis et al.*, 2005]. The potential hence exists to monitor sulfide mineral formation processes in marine environments and wetlands, remediation of mine wastes using wetlands, and biostimulation strategies for the degradation of contaminants.

[3] The spectral induced polarization (SIP) method measures the low-frequency (sub-kHz) electrical properties (related to both conduction loss and charge storage) of a porous medium (see *Lesmes and Friedman* [2005] for review). The method was developed for locating buried mineral deposits (e.g. massive FeS mineralization) based on a polarization phenomenon occurring at the interface between metallic minerals and pore-filling fluid [*Wong*, 1979]. *Williams et al.* [2005] showed that the formation of FeS biominerals under sulfate reducing conditions generates measurable (~15 mrad) SIP signals with central relaxation frequencies between 0.1–10 Hz. *Ntarlagiannis et al.* [2005] analyzed single frequency data from the same experiment and showed that the polarization magnitude is proportional to the rate of microbial activity.

[4] In this letter we extend this work by reporting results of a new column experiment whereby we first induce anaerobic FeS biomineralization but then subsequently induce biomineral dissolution by returning the system to an oxic state. We also model the SIP signature of both phases using a Cole-Cole relaxation [*Cole and Cole*, 1941]. We show that the SIP signal (and modeled dispersion parameters) generated during biomineralization is fully reversible and exhibits no significant hysteresis. Furthermore, we show that the time constant of the relaxation (and its temporal behavior during biomineral formation and dissolution) is consistent with the source of this polarization being biomineral encrusted pores of the sand matrix, and not the biomineral encrusted bacterial cells themselves.

2. Methods

[5] Experiment materials (fluids, sand matrix, tubing] were autoclaved, with PVC column parts that were not autoclavable sterilized in ethanol (>95%). Quartzitic sand (grain size for which 50 % of sample is finer (d_{50}) = 0.3 mm; porosity = 37 ± 1 %), treated to remove trace organics and/or iron oxides, was packed into a horizontal column (diameter = 0.0317 m; length = 0.203 m) containing six Ag-AgCl electrodes housed in electrolyte-filled ports attached to the column edge. Two Ag-AgCl coils (diameter = 0.0317 m) were emplaced at column ends for current injection. The column was saturated and continually flushed with a growth medium (including lactate, sulfate, iron, minerals and vitamins) and purged with N_2 gas to remove residual air bubbles. A continuous flow rate of ~2 pore volumes/day (~0.4 m/day) was established with a peristaltic pump for 55 days. The growth medium entered the column through a dedicated port at the column center and exited it through ports on both column ends. We assume complete pore cycling during early experiment time but recognize the possibility of flow-bypassing of dead end zones as a result of heterogeneous biomineral formation. Between Days 0–35 (anoxic phase) the column was placed in an anerobic chamber to facilitate microbial sulfate reduction. The anaerobic cham-

[1]Department of Earth and Environmental Sciences, Rutgers University, Newark, New Jersey, USA.
[2]Now at School of Planning, Architecture and Civil Engineering, Queen's University Belfast, Belfast, UK.
[3]Lawrence Berkeley National Laboratory, Berkeley, California, USA.

0094-8276/07/2007GL031840$05.00

ber was opened to the atmosphere on Day 36 until Day 55 to encourage FeS oxidation and dissolution. The growth medium was still continuously circulated (without sparging with N_2) but exposed to air via a 0.45 μm filter.

[6] Cells of a pure culture of *Desulfovibrio vulgaris* (*D. vulgaris*) were grown and inoculated into the center of the experiment column via syringe on Day 5. Pore water samples for analysis of aqueous geochemistry were extracted by sterile syringe (new syringe on each occasion) at three sampling ports equipped with rubber septa and equally spaced along the column, every 1–2 days following inoculation. We measured Eh, pH, and electrolyte conductivity using bench-top probes. Lactate, acetate, and sulfate were measured with an ion chromatograph. Hydrogen sulfide (H_2S) concentration was estimated using a test kit (HACH HS-WR) immediately after sampling to minimize volatization of H_2S to the atmosphere. The column solid phase was analyzed upon termination of the experiment at Day 55 using scanning electron microscopy (SEM). Columns were protected from sunlight throughout the experiment to minimize ultraviolet effects that could induce fungal growth.

[7] SIP measurements were collected at 40 equally spaced (in log space) frequencies between 0.1–1000 Hz using a dynamic signal analyzer (see *Slater and Lesmes* [2002] for details). Current was applied via the coil electrodes, and impedance magnitude and phase shift (φ) recorded relative to a precision resistor. This measurement was made at three locations along the column (between electrode pairs 1–2, 3–4, and 5–6) at 1–3 day intervals. The measurement error for the magnitude is less than 1% whereas the error in φ is ~0.1 mrad below 100 Hz [*Slater and Lesmes*, 2002].

[8] The SIP datasets were modeled with a phenomenological Cole–Cole dispersion expressed in terms of a complex resistivity (ρ^*),

$$\rho^* = \rho_0\left[1 - m\left(\frac{1}{1 + (i\omega\tau)^c}\right)\right], \quad (1)$$

where ρ_0 is the dc resistivity, τ is the mean relaxation time associated with the frequency dispersion, c is a shape exponent (0.2–0.8 for unconsolidated soils) and m is the chargeability associated with the interfacial charge storage [*Pelton et al.*, 1978]. Model parameters were estimated using an algorithm employing a least-squares approach with Marquardt regularization [*Kemna*, 2000] that nests a second higher-frequency relaxation (usually to model coupling effects in field data). As the SIP frequency range is usually not wide enough to capture the shape of the second relaxation we only report the parameters for the primary relaxation here. We recognize that Cole-Cole parameter estimation based on the minimization of a cost function using a least-squares criterion is uncertain and may find local minima in the objective function. Bayesian approaches have recently been shown to provide a better approach to Cole-Cole parameter estimation [*Ghorbani et al.*, 2007]. However, analysis of parameter uncertainty suggested that τ is a well resolved parameter in our modeling (estimated variances being less than 8% of the parameter estimate) although the variances of the other parameters is considerably greater.

3. Results

[9] Figure 1a summarizes the aqueous geochemistry of the system (average values for the samples extracted from the three sampling ports along the column) over the 55 days of the experiment. We define three system states: (1) the anaerobic transition (t = 14–25 days); (2) the anaerobic phase (t = 26–35 days); and (3) the aerobic transition (t = 36–45 days). The anaerobic transition represents the onset of biomineralization (following a ~2–3 day lag phase) as evidenced by decreasing sulfate (electron acceptor), decreasing lactate (carbon source), increasing acetate (reaction byproduct) and increasing H_2S (reaction byproduct) due to sulfate reduction. The aqueous H_2S produced from microbial induced sulfate reduction, commonly reacts with any metals in solution forming metal sulfides (solid state). In our column the dominant metal in solution is Fe^{2+} (125 μm inflow concentration) and the precipitating sulfide is FeS,

$$Fe^{2+} + H_2S_{(aq)} \rightarrow FeS_{(s)} + 2H^+. \quad (2)$$

[10] The anaerobic phase is characterized by relatively stable, low levels of lactate and sulfate but high levels of acetate and H_2S. This phase represents maximum rates of microbial activity and coincided with maximum visible precipitate formation, interpreted to be $FeS_{(s)}$. The black precipitate was visible through the clear column casing by Day 10 and confirmed, by SEM supported with Energy Dispersive X-ray (EDX) imaging of samples extracted at the end of the experiment, as FeS biomineralization.

[11] The aerobic transition represents the return of the system to oxic conditions. Oxidation of FeS over a ~10 day period (Day 36–45) is supported by previous laboratory studies confirming rapid rates of pyrrhotite ($Fe_{(1-x)}S$, $0.0 < x < 0.125$) oxidation at atmospheric concentrations of O_2 and at 22° C, being ~100 times those measured for pyrite (FeS_2) [*Nicholson and Scharer*, 1994]. The decline in sulfide after Day 36 can be attributed to an increase in its oxidation by oxygen, thus supporting a successful aerobic transition. Evidence of both low levels of lactate and SO_4^{2-} during the aerobic state suggests that anaerobic sulfate reduction was sustained throughout the experiment. This is consistent with the known tolerance of *D. vulgaris* in microaerophillic (even in aerobic) conditions, it being likely that cells survived the aerobic transition, albeit with reduced activity. The aerobic transition was directly visible from the disappearance (dissolution) of the FeS precipitate.

[12] In the interest of brevity we present only the results for electrode pair 5–6 here. Electrode pairs 1–2 and 3–4 displayed very similar behavior except that the maximum phase peaks were only 3 mrad, compared to 8 mrad for pair 5–6. A full analysis of the complete geoelectrical dataset will be presented in a forthcoming paper. Consistent with the results of *Williams et al.* [2005], FeS biomineralization results in the development of a dispersive relaxation. Figure 1b is a plot of resistivity magnitude ($|\rho|$) and phase (φ) as a function of frequency at t = 21 days (anaerobic

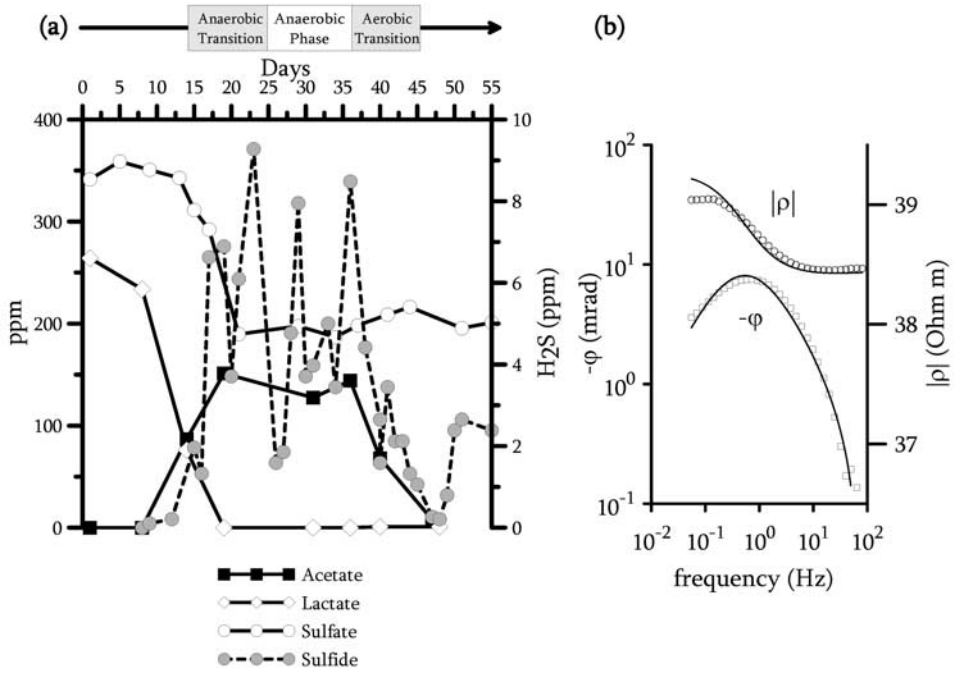

Figure 1. (a) Column aqueous geochemistry. Anaerobic and aerobic transitions when SIP data were collected are shaded. Lactate, acetate and sulfate are plotted on the left y-axis whereas sulfide is plotted on the right y-axis. (b) SIP signature of biomineralization at 21 days showing both phase (φ) and magnitude ($|\rho|$). Open symbols, measured data; Solid lines, Cole-Cole model fit (ρ_0 = 39.1 Ohm m; m = 0.025; τ = 0.22 s; c = 0.76). The RMS misfit between the model and measured data is 9%.

transition) illustrating this dispersion and showing the fit of Equation 1. The data are truncated at 100 Hz as above this frequency φ is less than the instrument accuracy (0.1 mrad). The open squares/circles are the measurements, and the lines depict the dispersion model fit. The model fits the data well (RMS error between model and data = 9%) except below 0.1 Hz (most obvious in the $|\rho|$ term due to the fine plotting scale), which may suggest the presence of a low frequency relaxation just captured in this dataset. The

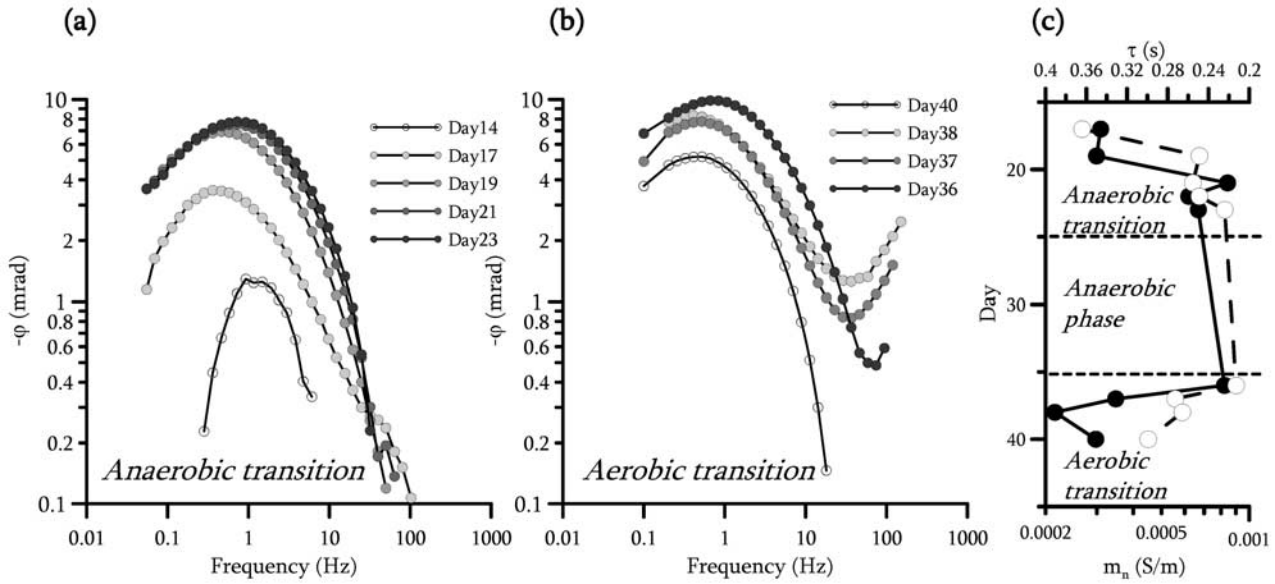

Figure 2. Measured phase ($-\varphi$) data as a function of time (a) Anaerobic transition. (b) Aerobic transition. The data are truncated at a value of -0.1 mrad (the accuracy of the instrument). (c) Variation of modeled Cole-Cole parameters as a function of time (black circles, τ; open circles, m_n).

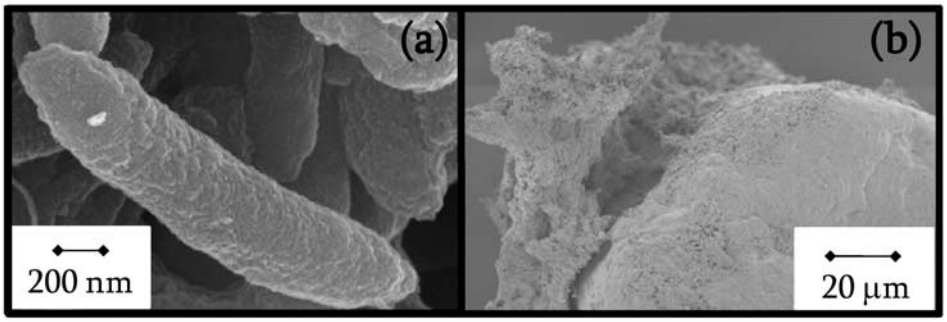

Figure 3. Examples of SEM images for samples extracted from the column on termination of experiment (Day 55). (a) Tube-like, elongate *D. vulgaris* biomineral with dimensions of 1.93 + −0.15 μm by 0.44 + −0.06 μm (based on three cells captured in three separate images). (b) Quartz sand particle encrusted with biomineralization.

modeled time constant for the primary relaxation is 0.22 s (see Figure 1 caption for other parameters).

[13] The temporal character of the SIP signature of this biomineralization process is demonstrated for the anaerobic transition and aerobic transition stages in Figure 2a and 2b, respectively. Data points where $\varphi < 0.1$ mrad are again omitted. Figure 2c shows the temporal evolution of the estimated dispersion model parameters $m_n = m/\rho_0$ (being the polarization strength [e.g., *Lesmes and Frye*, 2001]) and τ obtained for these datasets. Note that a satisfactory model could not be fit to the Day 14 dataset due to the very small polarization peak ($\sim$1.5 mrad). The anaerobic transition is characterized by an increase in the dispersion strength (i.e. increase in phase peak in data and m_n from model) and shift in phase peak to higher frequencies (decrease in τ from model). The aerobic transition shows essentially the reverse behavior as evidenced in the data (Figure 2b) and the modeled parameters (Figure 2c).

[14] Post experimental destructive analysis (Day 55) followed by SEM imaging indicated the presence of biominerals (Figure 3a) and biofilms on quartz grains (Figure 3b). The SEM-EDX analysis showed that both biominerals and biofilms are composed of FeS. The FeS encrusted cells (Figure 3a) show the characteristic curved rod shape of *D. vulgaris* with an average size of 0.44 ± 0.06 μm and 1.93 ± 0.15 μm (based on three SEM images) in the short and long axis, respectively.

4. Discussion

[15] The SIP response of FeS biomineralization can be modeled with a Cole-Cole model with τ in the range of 0.2–0.4 s (Figure 2c). We find that the SIP response that develops during the transition to sulfate reducing conditions and biomineral formation (anaerobic transition) is reversible, exhibiting no significant evidence of hysteresis, upon biomineral dissolution during return to oxic conditions (aerobic transition). This suggests that the SIP method could be used to monitor and track not only variable rates, but also variable directions, of microbial-mineral transformations in environments where redox conditions fluctuate.

[16] Although purely a phenomenological approach, the Cole-Cole modeling affords insights into the polarization mechanism associated with this process. It is recognized that τ is inversely related to some measure of the length scale over which ions in the electrical double layer at the mineral-fluid interface are displaced. *Schwarz* [1962] provides a model for the polarization of a particle in a uniform electrical field, based on tangential ionic fluxes, whereby the time constant of the relaxation is related to the particle radius (r),

$$\tau = \frac{r^2}{2D}, \tag{3}$$

where D is the surface ionic diffusion coefficient (in m^2s^{-1}). Values of D are uncertain but are often considered to be an order of magnitude smaller than the diffusion coefficient for the bulk solution ($\sim 10^{-9}$ m^2s^{-1}).

[17] *Tarasov and Titov* [2007] performed SIP measurements on sands with a well defined, narrow grain size distribution and estimated D as $\sim 3 \times 10^{-9}$ m^2s^{-1}. Table 1 shows the equivalent polarizable particle diameter for the two end members of the modeled τ range shown in Figure 2c based on this value of D. The estimates (0.07–0.10 mm) are almost two orders of magnitude larger than the long axis (approaching three orders of magnitude larger than the short axis) of the FeS encrusted biominerals (Figure 3a). Despite the simplicity of the model (the tubular biominerals in Figure 3a are not spherical particles, uncertainty in the magnitude of D), this discrepancy suggests that the dispersion between 0.1–100 Hz is not the relaxation associated with polarized biomineral-encrusted bacterial cells themselves.

Table 1. Comparison of SIP Estimated Radii r of Polarizable Spheres With Sand Grain Size From Sieve Analysis and Biomineral Size From SEM Imaging

				Biomineral[d]	
D,[a] m^2 s^{-1}	τ, s	$2r$,[b] mm	Sand d_{50},[c] mm	Long Axis, mm	Short Axis, mm
3.00E-09[e]	0.4	0.10	0.30	0.0019	0.0004
3.00E-09	0.2	0.07		±0.0001[f]	±0.0001[f]

[a] After *Tarasov and Titov* [2007].
[b] Calculated from equation (3).
[c] From sieve analysis.
[d] From SEM images.
[e] Read 3.00E-09 as 3.00×10^{-9}.
[f] Calculated from standard deviation of measurements on three biominerals.

[18] The particle size estimated from Equation 3 is close to (about 3 times smaller than) the d_{50} of the quartzitic sand particles used in this study (Table 1). We therefore suggest that the SIP relaxation observed here (and by *Williams et al.* [2005]) likely results from the formation of FeS biofilms (coagulation of individual biominerals) on the mineral surface of pores in the sand matrix. An example of this FeS biofilm forming on a quartzitic sand grain is shown in Figure 3b. We thus interpret the basic polarizable element to be the biomineral encrusted pores, having similar dimensions to the grains.

[19] This polarizable pore model can conceptually explain the change in τ and m_n (or from the data, $1/f_c$ and magnitude of phase peak) observed during the anaerobic, and subsequent aerobic, transitions. The variation in m_n is consistent with this model as m_n is a measure of the amount of polarizable surface area [*Lesmes and Friedman*, 2005]. The increase in m_n during the anaerobic transition is consistent with an increase in FeS-fluid interfacial area resulting from biomineralization growth within the pore space. The reverse behavior during the subsequent aerobic transition is then expected given the subsequent biomineral dissolution and loss of FeS-pore fluid interfacial area. The decrease in τ (and hence r) during the anaerobic transition is consistent with a shift to a smaller average polarizable pore size as the FeS lining the pores thickens. The reverse behavior is then observed in the aerobic transition as FeS dissolution starts at the biomineral-fluid interface and progressively enlarges the pores back to their original sizes. We note that such direct relation between τ and m_n could conceivably break down if FeS mineralization continued such that pores became so extensively filled with FeS that FeS-fluid interfacial area started to decline. Visual observations of the column (and flow rates) suggest that such extensive biomineralization was avoided.

[20] We conclude that SIP signatures are likely diagnostic of pore-scale geometrical changes associated with FeS biomineralization in pores by sulfate reducing bacteria. These signatures appear reversible (within the accuracy of the measurement) following subsequent biomineral dissolution. The estimates of polarizable element (i.e. biomineral-modified pore) size are uncertain, although this uncertainty may decrease using Bayesian estimation procedures [*Ghorbani et al.*, 2007]. Our work highlights the opportunity that exists to improve understanding of biogeochemical processes using geophysical measurements that could be deployed from boreholes or the ground surface.

[21] **Acknowledgments.** This study was funded by the Department of Energy, Environmental Remediation Sciences Program (ERSP) grant 1027674 to S. Hubbard. This material is also based upon work supported by the National Science Foundation under grant 0433739. Andreas Kemna provided the Cole-Cole relaxation modeling algorithm used here.

References

Atekwana, E., D. D. Werkema Jr., and E. Atekwana (2006), Biogeophysics: The effects of microbial processes on geophysical properties of the shallow subsurface, in *Applied Hydrogeophysics*, *NATO Sci. Ser.* IV, edited by H. Vereeken et al., pp. 161–193, Springer, New York.

Cole, K. S., and R. H. Cole (1941), Dispersion and absorption in dielectrics, vol. I. Alternating current field., *J. Chem. Phys.*, *9*, 341–351.

Ghorbani, A., C. Camerlynck, N. Florsch, P. Cosenza, A. Tabbagh, and A. Revil (2007), Bayesian inference of the Cole-Cole parameters from time and frequency-domain induced polarization, *Geophys. Prospect.*, *55*, 589–605, doi:10.1111/j.1365-2478.2007.00627.x.

Kemna, A. (2000), *Tomographic Inversion of Complex Resistivity—Theory and Application*, 176 pp., Der Andere, Osnabrück, Germany.

Lesmes, D. P., and S. P. Friedman (2005), Relationships between the electrical and hydrogeological properties of rocks and soils, in *Hydrogeophysics*, edited by Y. Rubin and S. S. Hubbard, pp. 87–128, Springer, Dordrecht, Netherlands.

Lesmes, D. P., and K. M. Frye (2001), The influence of pore fluid chemistry on the complex conductivity and induced-polarization responses of Berea sandstone, *J. Geophys. Res.*, *106*, 4079–4090.

Nicholson, R. V., and J. M. Scharer (1994), Laboratory studies of pyrrhotite oxidation kinetics, in *Environmental Geochemistry of Sulfide Oxidation*, *ACS Symp. Ser.*, vol. 550, edited by C. N. Alpers and D. W. Blowes, pp. 14–30, Am. Chem. Soc., Washington, D.C.

Ntarlagiannis, D., K. H. Williams, L. Slater, and S. Hubbard (2005), Low-frequency electrical response to microbial induced sulfide precipitation, *J. Geophys. Res.*, *110*, G02009, doi:10.1029/2005JG000024.

Pelton, W. H., S. H. Ward, P. G. Hallof, W. R. Sill, and P. H. Nelson (1978), Mineral discrimination and removal of inductive coupling with multi-frequency IP, *Geophysics*, *43*, 588–609.

Schwarz, G. (1962), A theory of the low-frequency dielectric dispersion of colloidal particles in electrolyte solution, *J. Phys. Chem.*, *66*, 2636–2642.

Slater, L., and D. P. Lesmes (2002), Electrical-hydraulic relationships observed for unconsolidated sediments, *Water Resour. Res.*, *38*(10), 1213, doi:10.1029/2001WR001075.

Tarasov, A., and T. Titov (2007), Relaxation time distribution from time domain induced polarization measurements, *Geophys. J. Int.*, *170*, 31–43.

Williams, K. H., D. Ntarlagiannis, L. Slater, A. Dohnalkova, S. S. Hubbard, and J. F. Banfield (2005), Geophysical imaging of stimulated microbial biomineralization, *Environ. Sci. Technol.*, *39*(19), 7592–7600.

Wong, J. (1979), An electrochemical model of the induced-polarization phenomenon in disseminated sulfide ores, *Geophysics*, *44*, 1245–1265.

S. Hubbard, Lawrence Berkeley National Laboratory, Earth Science, MS 90-1116 1 Cyclotron Road, Berkeley, CA 94720-0000, USA.

D. Ntarlagiannis, School of Planning, Architecture and Civil Engineering, Queen's University Belfast, Belfast BT7 1NN, UK.

Y. R. Personna and L. Slater, Department of Earth and Environmental Sciences, Rutgers University, 101 Warren Ave/Rm 142, Newark, NJ 07102-0000, USA.